Research Square

Preprints are preliminary reports that have not undergone peer review.
They should not be considered conclusive, used to inform clinical practice,
or referenced by the media as validated information.

Multi-Objective Gravity Data Inversion for Basement Depth Estimation in Sedimentary Basins

Ahmad A. Reza
Institut Teknologi Sepuluh Nopember
Silvia Lestari
Institut Teknologi Sepuluh Nopember
S. Sungkono
sungkono@its.ac.id

Institut Teknologi Sepuluh Nopember
S. Saifuddin
Institut Teknologi Sepuluh Nopember
Firman Syaifuddin
Institut Teknologi Sepuluh November
Juan P.G.N. Rochman
Institut Teknologi Sepuluh November
Ilham Arisbaya
National Research and Innovation Agency (BRIN), KST Samaun Samadikun
Khalid S. Essa
Cairo University

Research Article

Keywords: Gravity anomaly inversion, Multi-objective optimization, AMALGAM algorithm, basement depth estimation, sedimentary basin characterization, subsurface imaging

Posted Date: August 13th, 2026

DOI: https://doi.org/10.21203/rs.3.rs-10464871/v1

License: This work is licensed under a Creative Commons Attribution 4.0 International License.
Read Full License

Additional Declarations: Competing interest reported. The authors declare that there are no known competing financial interests or personal relationships that could have influenced the work presented in this paper.

Multi-Objective Gravity Data Inversion for Basement Depth Estimation in Sedimentary Basins

Ahmad A. Reza[1], Silvia Lestari[1], S. Sungkono[1*], S. Saifuddin[1], Firman Syaifuddin[2], Juan P.G.N. Rochman[2], Ilham Arisbaya[3], Khalid S. Essa[4]

[1]Departement of Physics, Faculty of Science and Data Analytics, Institut Teknologi Sepuluh Nopember, Surabaya 60111, Indonesia

[2]Department of Geophysical Engineering, Faculty of Civil, Planning, and Geoengineering, Institut Teknologi Sepuluh November, Surabaya, 60111, Indonesia

[3]Research Center for Geological Disaster, National Research and Innovation Agency (BRIN), KST Samaun Samadikun, Jl. Cisitu Sangkuriang, Bandung 40135, Indonesia

[4]Geophysics Department, Faculty of Science, Cairo University, Giza 12613, Egypt

*Corresponding Author:

E-mail address: sungkono@its.ac.id (Sungkono)

Abstract

Accurate estimation of basement depth is significant in the energy resource exploration and mineral prospecting. Basement depth is inherently controlled by a combination of sedimentation, tectonic subsidence, and geological processes that collectively shape the subsurface architecture. The reconstruction of basement depth and its density variations represents a valuable and well-established application of gravity anomaly inversion. Conventional approaches to generating geologically realistic basement models typically rely on regularization techniques, frequency-domain filtering methods, and smoothness constraints within optimization frameworks to stabilize

the inversion process. This study investigates the application of the adaptive multi-objective optimization algorithm (AMALGAM) for accurate characterization of sedimentary basin geometry. Within this optimization framework, gravity data inversion is formulated to simultaneously minimize two competing objective functions, namely, the data misfit term and the model smoothness constraint, thereby eliminating the need for post-inversion smoothing or spectral filtering of model parameters. The multi-objective optimization ensures that one objective does not over-dominate without applying weighting and regularization schemes. The result is an ensemble of non-dominated optimal solutions called the Pareto-optimal set. The robustness and reliability of the proposed algorithm are systematically evaluated and validated using both noise-free and noise-added synthetic gravity datasets. The algorithm's effectiveness is further demonstrated through its application to gravity anomaly data acquired over two real sedimentary basins. The results confirm that the proposed approach constitutes a promising, accurate, and computationally efficient method for subsurface imaging in geological and geophysical exploration.

Keywords: Gravity anomaly inversion, Multi-objective optimization, AMALGAM algorithm, basement depth estimation, sedimentary basin characterization, subsurface imaging.

1. Introduction

Sedimentary basins constitute a significant proportion of the Earth's surface and primarily formed as a consequence of tectonic activity. A sedimentary basin is broadly defined as a depression within the Earth's crust that undergoes progressive and relatively long-term subsidence over geological timescales. These structural depressions serve as repositories for large-scale sediment accumulation of varying geometries and dimensions on top of metamorphic or igneous basement rocks throughout geological history (Weissmann et al. 2015). The development of a

sedimentary basin is further supported by the accumulation of material resulting from erosion, chemical deposition, and organic remains in the aquatic environment (Onajite 2013). Over millions of years, complex interactions among organic material, sediment deposits, and water give rise to economically significant energy resources, including hydrocarbon, geothermal energy, and groundwater reserves. Consequently, accurate estimation of basement depth within sedimentary basins is crucial in a wide range of energy resource exploration. These include the identification of structural traps and stratigraphic configuration for oil and gas exploration, hydrogeological investigation, and geothermal resource evaluation (Harding and Tuminas 1989; Bohidar et al. 2001; Pamukçu et al. 2019; Lyu et al. 2023; Panthi et al. 2023; Peng et al. 2025).

Basement depth estimation is commonly achieved through gravity anomaly inversion, which is inherently a non-linear problem. The unknown model parameters correspond to the basement depths at each observation point, rendering the high-dimensional problem in nature. Previous studies have developed techniques to solve the inversion problem. Non-linear inversion problems have been addressed using local optimization methods, which depend on the gradient of the objective function, including Bott's iterative approach (Bott 1960), the Gauss-Newton method (Silva et al. 2014), and the total variation approach (Santos et al. 2015). However, local optimization methods are inherently susceptible to entrapment local minima, which poses a significant challenge given that geophysical inversion problems are predominantly non-linear in character. On the other hand, gravity inversion is both ill-posed and non-unique in nature, meaning that multiple subsurface models may produce the same gravity response on certain error bounds (Pallero et al. 2015, 2017, 2021; Jamasb et al. 2017, 2019; Ekinci et al. 2021; Roy et al. 2021b, a). This inherent non-uniqueness implies a diverse range of basement depth and geometry models may equally match the observed gravity anomalies. As a result, any single solution is insufficient

to adequately represent the entire geologically reasonable models within the model space (Fernández Martínez et al. 2012; Fernández-Martínez et al. 2013, 2014a).

Various approaches have been proposed to mitigate the non-uniqueness inherent in gravity inversion, most notably the incorporation of prior geological information and the introduction of additional regularization functions aimed at constraining the solution space and reducing the number of admissible models (Barbosa et al. 1997, 1999; Jamasb et al. 2017). Although such approaches are effective in narrowing the range of plausible solution, numerous studies have demonstrated that regularization does not entirely eliminate solution equivalence; rather it, selectively identifies a single solution from among the many geologically feasible alternatives (Fernández-Martínez et al. 2014b, a). This may lead to misinterpretation, particularly when the prior information is founded on geological assumptions that may not accurately reflect true subsurface condition. Moreover, the quality and stability of the resulting solution are highly sensitive to the choice of the regularization parameter, which introduces an additional layer of subjectivity into the inversion process (Horikawa and Kusumoto 2025). A further limitation of gradient-based local optimization methods is that the model update at each iteration is computed from the first-order derivative of the objective function with respect to the model parameters, while may not be analytically computable in certain geophysical inversion scenarios (Jamasb et al., 2017, 2019).

Global optimization methods have been widely applied in geophysical inversion problems to overcome the inherent limitations associated with local optimization techniques and regularization. Several global optimizations have been successfully applied to non-linear and multimodal geophysical data inversion problems, including the Genetic Algorithm (GA) (Xing and Mazzotti 2019), Particle Swarm Optimization (PSO) (Pallero et al. 2021; Roy et al. 2021a),

Simulated Annealing (SA) (Biswas and Acharya 2016), Differential Evolution (DE) (Sungkono 2020; Ekinci et al. 2021; Roy et al. 2021b), Imperialist Competitive Algorithm (ICA) (Joolaei et al. 2022), Runge-Kutta optimization (Ramadhan et al. 2024), Rao algorithm (Warnana et al. 2025), Jaya algorithm (Saifuddin et al. 2025), Generalized Normal Distribution Optimization (Sungkono et al. 2025), and Bat algorithm (Essa et al. 2025b, a). Unlike local optimization methods, global optimization methods are not dependent on the initial guess or model, possess the capacity to explore broad and complex parameter space, and are capable of escaping local minima. These characteristics render them particularly well-suited for gravity inversion application aimed at basement depth estimation (Ekinci et al. 2021; Pallero et al. 2021; Roy et al. 2021b; Joolaei et al. 2022). However, existing global optimization applications to gravity inversion have still been formulated within a single objective function, in which the data misfit and regularization terms are combined into a composite objective function through a weighted sum approach (Jamasb et al. 2017, 2019). This approach has a fundamental drawback, as the Lagrange multiplier (regularization parameter) selection is inherently subjective, either through trial-and-error procedures or a certain value is used as search bounds and optimized it simultaneously with basement depth parameters. The selected regularization parameter then can significantly influence the final inversion outcome (Fernández-Martínez et al. 2014b, a; Jamasb et al. 2017; Lestari et al. 2026).

Multi-objective optimization (MOO) is a convenient solution because both model fitting and regularization are treated as two separate and independent functions that compete with each other. The outcome of such an approach is a set of mutually non-dominated optimal solutions called the Pareto front (PF) within in the objective space (Deb et al. 2002b; Vrugt and Robinson 2007). In this framework, an improvement in one objective is generally accompanied by

degradation in the other, such that each point along the Pareto front reflects a distinct and meaningful trade-off between the competing objectives. Despite some additional analyses and interpretations, the MOO approach provides substantially information about the range of acceptable solutions and its uncertainty (Akca et al., 2014; Bijani et al., 2017; Dal Moro, 2008; Dal Moro & Pipan, 2007).

While MOO methods offer significant advantages for solving multi-objective geophysical inversion problems, it is important to recognize that individual algorithms differ markedly in their exploration and exploitation characteristics, as well as their sensitivity to topology of objective function landscape. This observation is formally encapsulated by the No Free Lunch Theorem (NFL), which establishes that no single optimization algorithm can outperform all others across the full range of optimization problems (Wolpert and Macready 1997). Consequently, relying on a single algorithm may potentially constrain the capacity to identify globally optimal solutions, especially for high-dimensional and multimodal, and inherently non-linear inversion problems (Vrugt and Robinson 2007; Vrugt et al. 2009).

To overcome these limitations, A Multi-Algorithm Genetically Adaptive Multi-objective method (AMALGAM) was developed as an evolutionary-based multi-objective optimization algorithm that implements the concept of adaptive multi-method search. AMALGAM simultaneously integrates multiple search strategies with complementary exploration and exploitation characteristics, enabling a more comprehensive and flexible traversal of the solution space. Each constituent algorithm contributes to offspring production at each generation, allowing the population to evolve in parallel through multiple search mechanisms. The key feature of AMALGAM is its reproductive success-based adaptation mechanism, where the proportional contribution of each constitute search method is dynamically adjusted according to its relative

effectiveness in generating Pareto-optimal solutions in preceding generations. Specifically, search strategies that demonstrate superior performance are assigned a higher selection probability in the next generation, while less effective strategies have their contribution gradually reduced, though not completely eliminated, from the search process. This adaptive scheme allows AMALGAM to automatically adjust its search behaviour in response to the geometry and complexity of the objective function landscape, achieving a dynamic balance between exploration and exploitation without requiring manual parameter tuning (Vrugt and Robinson 2007; Vrugt et al. 2009; Vrugt 2015). Previously, AMALGAM has been successfully applied to geophysical inversion problems, demonstrating its utility in hydrogeological model parameterization derived from Electrical Resistivity Tomography (ERT) and Time Domain Reflectometry (TDR) data (Huisman et al. 2010). This prior application substantiates the potential of AMALGAM as a robust and versatile framework for addressing a broader range of geophysical inversion problems.

In this study, AMALGAM is applied to gravity anomaly inversion for the purpose of estimating the basement depth of a sedimentary basin. Instead of finding a single optimal solution, the proposed inversion framework yields a set of Pareto-optimal solutions that represent various trade-offs between data misfit and model complexity. This formulation enables a more rigorous and systematic assessment of model uncertainty while substantially mitigating the adverse effects of solution non-uniqueness inherent in gravity inversion problems. The performance of the proposed approach is evaluated through its application to both synthetic and field gravity anomaly datasets, against which its computational efficiency, robustness, and inversion accuracy are thoroughly assessed.

2. Forward Modelling

Several parameterization models have been proposed for gravity inversion of basement relief in sedimentary basins. Among these, a widely adopted approach involves computing the cummulative gravity fields of a series of juxtaposed two-dimensional prisms to approximate the basement relief geometry (Telford et al. 1990; Barbosa et al. 1997; Pallero et al. 2015). In this formulation, both the basement and the overlying sedimentary layer are assumed to be homogeneous in terms of density, and the thickness of each prism is treated as an unknown parameter to be recovered through the inversion process. A two-dimensional (2D) complex subsurface structure can be discretized into a variable number of adjacent rectangular blocks with limited vertices (Figure 1). As illustrated, seven juxtaposed vertices are employed to approximate the geometry of the true subsurface model. It is worth noting that increasing the number of vertices enhances the spatial resolution of the discretization, yielding a progressively closer approximation of the actual subsurface structure.

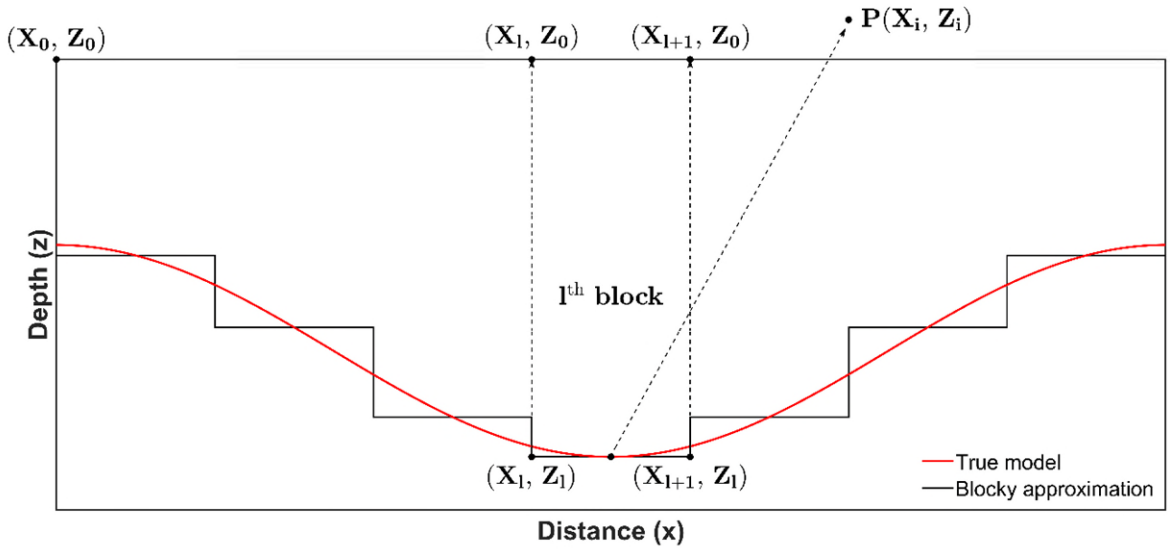


Figure 1 Discretization of the sedimentary basin geometry using a block rectangular prism approximation (Roy et al. 2025).

The vertical component of the gravitational attraction produced by a polygonal body discretization with L vertices at any given observation point $\left(P(x_i, z_i)\right)$ can be expressed as follows (Pallero et al. 2015; Roy et al. 2025):

$$\boldsymbol{g_z}(x_i, z_i) = G\Delta\rho \sum_{i=1}^{L-1} \left[A\, ln\left(\frac{A^2+D^2}{A^2+C^2}\right) - B\, ln\left(\frac{B^2+D^2}{B^2+C^2}\right) - 2C\left(tan^{-1}\left(\frac{A}{C}\right) - tan^{-1}\left(\frac{B}{C}\right)\right) + 2D\left(tan^{-1}\left(\frac{A}{D}\right) - tan^{-1}\left(\frac{B}{D}\right)\right)\right] \quad (1)$$

where $A = x_i - x_l$; $B = x_i - x_{l+1}$; $C = z_i - z_0$; and $D = z_i - z_l$; G indicates Newton's gravity constant, and $\Delta\rho$ represents density contrast between the sediment fill and the basement rock for each prism. Both x_l and x_{l+1} are horizontal locations for the minimal and maximal prisms, while z_l and z_0 denote the vertical locations for the top and bottom of the prims, respectively, as shown in Figure 1. Both x_i and z_i coordinates reflect the observation point.

3. Gravity Data Inversion Using Multi-objective Approach

3.1 The AMALGAM algorithm

The adaptive multi-objective optimization algorithm (AMALGAM) employs multiple evolution multi-objective optimizers (EMOs) concurrently and adaptively to ensure a fast, reliable, and computationally efficient solution to multi-objective optimization problems (Vrugt and Robinson 2007). In the initial step, AMALGAM generated a random initial parameter set (initial population) P_i with a population number N using the Latin Hypercube Sampling (LHS) method. The LHS-based initialization method effectively avoids the problems associated with local optimizations. The subscript i of P_i refers to the iteration number, ranging from 0 to the maximum number of iterations T. Subsequently, an offspring population $\bar{P}_i$ of size N is created by implementing each candidate algorithm within AMALGAM to produce a prescribed number of

offspring parameter solutions, $N = \{N_i^1, N_i^2, \cdots, N_i^k\}$, from P_i, where k denotes the ID of each candidate EMO within AMALGAM. The best N solutions within $R_i = P_i \cup \bar{P}_i$ are then selected into P_{i+1} using the fast non-domination sorting (FNS) approach (Deb et al. 2002b), which is repeatedly produced by the multi-method search and adaptive offspring creation method until the maximum number of iterations is satisfied.

AMALGAM has two key procedures: simultaneous multi-method search and self-adaptive offspring generation. In the multi-method search procedure, AMALGAM dynamically adjusts the number of parameter solutions contributed by each constituent EMO to the offspring population based on its current performance at each iteration. In the present implementation, AMALGAM integrates four EMO algorithms: the Non-dominated Sorting Genetic Algorithm (NSGA-II) (Deb et al. 2002b), Particle Swarm Optimization (PSO) (Kennedy and Eberhart 1995), Adaptive Metropolis Search (AMS) (Haario et al. 2001), and Differential Evolution (DE) (Storn and Price 1997). Within the NSGA-II, binary crossover approach (Deb and Agrawal 1995) and real mutation method (Deb et al. 2002a) are applied to the offspring population. The number of offspring points produced by each constituent algorithm ($\{N_i^1, N_i^2, \cdots, N_i^k\}$) is updated at every iteration based on Eq. (2) as follows:

$$N_i^k = N \times \left(O_i^k / N_{i-1}^k\right) / \sum_{n=1}^{k} \left(O_i^k / N_{i-1}^k\right) \quad (2)$$

where O_i^k / N_{i-1}^k refers to the ratio of the number of offspring points provided by the algorithm to the new population $\left(O_i^k\right)$ and the corresponding number produced by the algorithm in the previous generation $\left(N_{i-1}^k\right)$. For the first generation, $N_0^1 = N_0^2 = \cdots = N_0^k = N/K$, where K denotes the number of EMO candidates applied in the AMALGAM. The minimum value of N_i^k was $0.05 \times N$. Additionally, the AMALGAM algorithm requires N populations to calculate the forward modeling

and objective function for each iteration. Then, for T as the maximum iteration, AMALGAM requires $N \times T$ for the forward modeling and objective function calculation.

AMALGAM is designed to generate an ensemble of mutually non-dominated parameter solutions rather than converging toward a single optimal solution. A parameter solution is considered non-dominated when no other solution in the population is superior to it across all the objective functions simultaneously. More details about AMALGAM are available in the literature (Vrugt et al. 2003; Vrugt and Robinson 2007; Vrugt 2015). While the application of multi-objective optimizers and the concept of non-dominance in geophysical inversion have been explored in prior studies (Dal Moro and Pipan 2007; Dal Moro 2008; Xiong and Zhang 2015), a detailed treatment of these concepts is beyond the scope of the present work.

3.2 Objective functions

The intrinsic ill-posedness of the non-linear gravity inversion problem is that multiple subsurface models are capable to produce the observed gravity data with equivalent objective function values. To reduce the dimensionality of this solutions space and constrain the range of models that adequately fit the observed data, various forms of geological and mathematical constraints are typically imposed during the inversion process (Barbosa et al., 1997; Pallero et al., 2015). The incorporation of relative constraints within global search methods effectively limits the search domain to geologically feasible subset of the full model space, thereby guiding the inversion toward physically meaningful solutions (Ekinci et al. 2021).

In previous studies, the Lagrange multiplier approach has been widely employed to estimate realistic basement depth from gravity data inversion using metaheuristic algorithms (Jamasb et al. 2017, 2019; Roy et al. 2021b, a). However, the incorporation of a Lagrange multiplier within the objective function introduces a fundamental methodological limitation, as its

value is typically determined through subjective trial and error procedures, rendering the inversion outcome highly dependent to the chosen Lagrange multiplier value. Furthermore, in conventional single-objective inversion frameworks, the model is either spatially smoothed (Ekinci et al. 2021; Joolaei et al. 2022) or filtered (Pallero et al. 2015, 2021) before evaluating the objective function.

A multi-objective optimization algorithm commonly optimizes two or more objective functions using a combination of non-dominated sorting and crowding distance methods (Deb et al. 2002b) or alternatively through a decomposition-based approach population selection in successive iterations (Zhang and Li 2007). The multi-objective inversion framework adopted in this study has successfully minimized both data misfit and model constraints simultaneously in transient electromagnetic inversion (An et al. 2025) and two-dimensional magnetic inversion (Xiong and Zhang 2015). Thus, in this study, we applied the multi-objective method AMALGAM to invert gravity data to determine the basement depth. AMALGAM optimizes the model parameters by simultaneously minimizing two objective functions, as shown in Eq. (3)

$$min\{F(\boldsymbol{z})\} = \begin{bmatrix} F_1(\boldsymbol{z}) \\ F_2(\boldsymbol{z}) \end{bmatrix} \tag{3}$$

where $F_1(\boldsymbol{z})$ is the first objective function quantifies the misfit between the observed and calculated gravity anomaly data and is mathematically described as follows (Roy et al. 2021a):

$$F_1(\boldsymbol{z}) = \frac{\|\Delta \boldsymbol{g}_{obs} - \Delta \boldsymbol{g}_{calc}(\boldsymbol{z})\|_2}{\|\Delta \boldsymbol{g}_{obs}\|_2} \times 100\% \tag{4}$$

where $\Delta \boldsymbol{g}_{obs}$ denotes the observed gravity data, $\Delta \boldsymbol{g}_{calc}(\boldsymbol{z})$ is the calculated gravity data caused by the basement depth $\boldsymbol{z}$, and $\|\cdots\|_2$ indicates the L2-norm. The second objective $F_2(\boldsymbol{z})$ is the model constraint in the form of a roughness or smoothness regularization term, the imposition of which serves to reduce solution uncertainty and narrow the range of geologically admissible models (Fernández-Martínez et al. 2014b). $F_2(\boldsymbol{z})$ is defined by the following equation:

$$F_2(\boldsymbol{z}) = \frac{1}{M}\|\boldsymbol{D}_2\boldsymbol{z}\|_2 \quad (5)$$

where M indicates the number of model parameters, and $\boldsymbol{D}_2$ denotes the square matrix of the second-order difference operators. The L2-norm in Eq. (5) is utilized to smooth the basement depth (Martins et al. 2011; Lima et al. 2011). Furthermore, the $\boldsymbol{D}_2$ can be expressed as follows:

$$\boldsymbol{D_2} = \begin{bmatrix} 1 & -2 & 1 & 0 & \cdots & 0 \\ 0 & 1 & -2 & 1 & \cdots & 0 \\ \vdots & \vdots & \ddots & \ddots & \ddots & \vdots \\ 0 & 0 & \cdots & 1 & -2 & 1 \end{bmatrix} \quad (6)$$

3.3 Search space of the basement depth

Before applying the AMALGAM algorithm to the gravity data inversion process, it is necessary to define the boundary constraints of the model parameters search space. This step is essential to confine the optimization process exclusively to geologically realistic regions of the solution domain. In the context of two-dimensional basement relief estimation problems, the model parameters are represented as a vector of basement depths associated with each discretized cell or prism (Joolaei et al., 2022; Pallero et al., 2015). Therefore, the search space is defined by specifying the minimum and maximum permissible depth values for each individual model parameter. As an initial estimate, the basement depth at the i^{th} prism $(i = 1, 2, \ldots, M)$, defined by $z_i^{(0)}$, is calculated from the observed gravity anomaly values using the Bouguer slab approximation, expressed as follows (Pallero et al. 2015; Ekinci et al. 2021):

$$\boldsymbol{z_i^{(0)}} = \frac{\Delta g_{obs}}{2\pi G \Delta\rho} \quad (7)$$

where Δg_i^{obs} is the observed gravity data, G represents the universal gravitational constant, and $\Delta\rho$ is the density contrast between the sediment and the basement. The lower ($\boldsymbol{z_k^{min}}$) and upper ($\boldsymbol{z_k^{max}}$) bounds for the search space are determined using Eq. (8) (Pallero et al. 2015)

$$\left[\boldsymbol{z_k^{min}}, \boldsymbol{z_k^{max}}\right] = \left[k_{min}.\, z_i^{(0)}, k_{max}.\, z_i^{(0)}\right] \quad (8)$$

where $k_{min} < 1$ dan $k_{max} > 1$ to manage search space ranges.

4. Synthetic Studies

The multi-objective optimization approach based on AMALGAM was tested and evaluated using two synthetic basement depth models under both noise-free and Gaussian noise-added conditions. The use two structurally distinct synthetic models is intended to assess the algorithm's capacity to accurately reconstruct variations in basement geometry across a range of structural conditions, as well as to evaluate the stability of the inversion solutions with respect to increasing model complexity. The first model, namely Model 1, depicts a simple sedimentary basin composed of 50 prisms, each with a horizontal extent 1,000 m, characterized by a relatively smooth and laterally symmetrical depth variation, as shown in Figure 2. The second model called Model 2 represents a structurally more complex basin composed of 50 prisms, each with a horizontal extent of 100 m, featuring a more irregular basement relief that incorporates two depressions of contrasting depths (Figure 3). In both models, the density contrast between the crystalline basement and the overlying sediment fill is prescribed as -400 kg/m^3.

To simulate real-world conditions more accurately, a noise level was purposefully added to both synthetic datasets. This procedure is essential for assessing the robustness and stability of the inversion method under realistic conditions, where measurements are inherently subject to various sources of noise and uncertainty. The noise-added synthetic gravity data were generated according to the following expressions:

$$gN_{syn} = g_{syn} + NR \times mean\left(g_{syn}\right) \times randn\left(size(M)\right) \quad (9)$$

where g_{syn} represents the noise-free synthetic gravity data, $randn$ generates arrays of random values normally distributed between [-1, 1] of a given size of model parameters M, and $mean(g_{syn})$ indicates the average value of the synthetic data. The NR refers to the amount of random noise added, which was set to 10%.

The AMALGAM algorithm parameters have been applied to obtain fast and robust results for synthetic gravity data inversion (Vrugt and Robinson 2007). Specifically, the maximum number of iterations T for the inversion process was set to 100, and the population size N was set to 500. The search space boundaries for the basement depths were determined as in Eq. (8) with $k_{min} = 0.5$ and $k_{max} = 2.0$ based on previous literatures (Pallero et al. 2015; Ekinci et al. 2021; Joolaei et al. 2022).

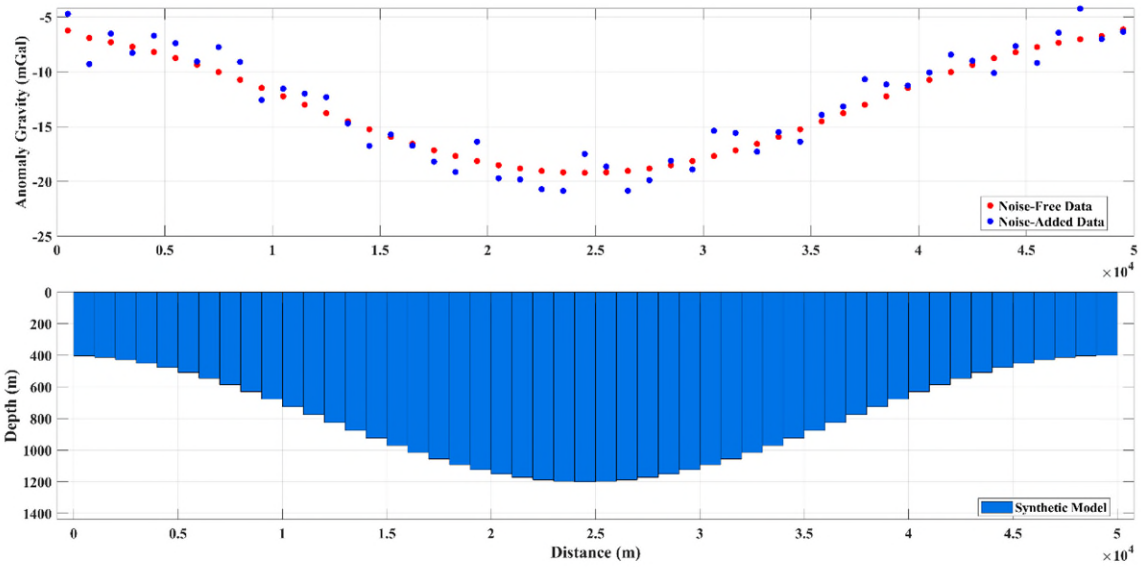


Figure 2 The 2D sedimentary basin of Model 1 and its associated gravity anomalies. Upper panel: Gravity anomalies computed from the synthetic basement depth for the noise-free (red dots) and noise-added (blue dots) cases. Lower panel: The synthetic model is divided into a series of 50 rectangular prisms with a uniform horizontal width of 1,000 m and a density contrast of -400 kg/m^3.

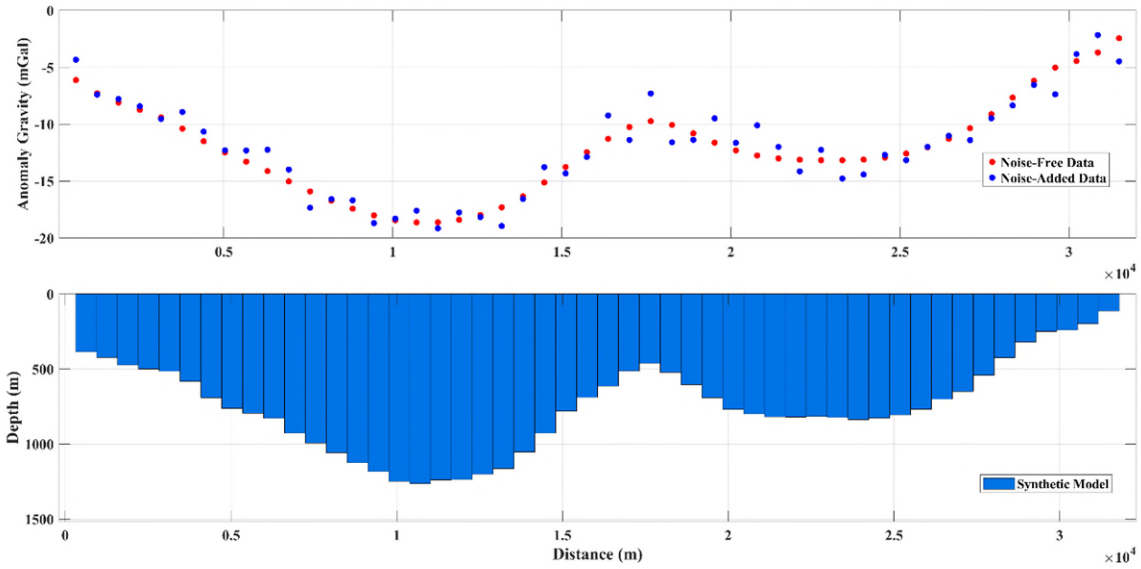


Figure 3 The 2D sedimentary basin of Model 2 and its associated gravity anomalies. Upper panel: Gravity anomalies computed from the synthetic basement depth for the noise-free (red dots) and noise-added (blue dots) cases. Lower panel: The synthetic model is divided into a series of 50 rectangular prisms with a uniform horizontal width of 100 m and a density contrast of -400 kg/m^3.

4.1 Noise-free

This section explains the result inferred from the proposed method in solving noise-free gravity anomaly data from Models 1 and 2. Figure 4 (a) and (b) show the evolution of $F_1(\boldsymbol{z})$ and $F_2(\boldsymbol{z})$ from the gravity inversion of the noise-free data case for Model 1, indicating that both objective functions decrease within the iteration. The Pareto front (PF) recorded at every 10 generations and the last iteration of PF are shown in Figure 4 (c), which indicates that no absolute best model can be defined from the PF. Finally, Figure 4 (d) presents the selection probability of each constituent algorithms (AMS, PSO, GA, and DE) across successive generation, revealing that the AMS, DE, and GA algorithms have higher probabilities than the PSO algorithm.

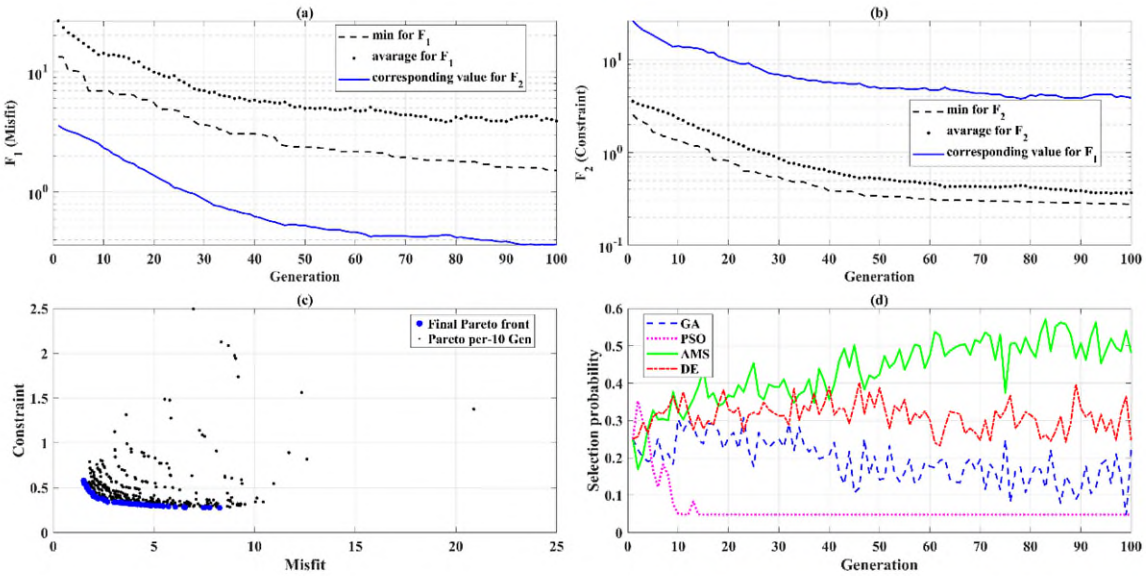


Figure 4 AMALGAM inversion results for noise-free gravity data inversion of Model 1: (a) Evolution of the first objective function $F_1(\boldsymbol{z})$ over successive generations; (b) Evolution of the second objective function $F_2(\boldsymbol{z})$ over successive generations; (c) Progression of the Pareto front (PF) in the objective space across generations; (d) Selection probability of each constituent algorithm (AMS, PSO, GA, and DE) per generation.

Table 1 Statistical summary of $F_1(\boldsymbol{z})$ and $F_2(\boldsymbol{z})$ values from inversion results of Model 1 and Model 2 with noise-free and noise-added conditions.

Objective Function	**Statistics Parameters**	**Model 1**		**Model 2**	
		Noise Free	**Noise-Added**	**Noise Free**	**Noise-Added**
Data misfit $(F_1(\boldsymbol{z}))$	Minimum	1.51	4.68	1.12	7.04
	Mean	3.48	6.27	2.79	7.98
	Median	3.23	6.04	2.27	7.64
	Maximum	8.26	9.73	7.85	11.69
	Standard Deviation	1.71	1.14	1.49	1.08
Model constraint $(F_2(\boldsymbol{z}))$	Minimum	0.28	0.36	0.38	0.51
	Mean	0.37	0.88	0.45	0.81
	Median	0.34	0.81	0.45	0.71
	Maximum	0.58	2.00	0.64	1.67
	Standard Deviation	0.08	0.37	0.06	0.27

The statistical summary of data misfit value $F_1(\boldsymbol{z})$ and model constraint value $F_2(\boldsymbol{z})$ across the Pareto-optimal solutions is presented in Table 1. In the noise-free data case, both Models 1 and 2 yield low standard deviation values, indicating that the results have good value distribution of objective functions. Figure 5 shows the PF obtained for both the Model 1 and Model 2 for under noise-free conditions. The PF contains several model parameter solutions that collectively constitute the set of admissible gravity data inversion outcomes, each characterized by a specific combination of data misfit $F_1(\boldsymbol{z})$ and model constraint $F_2(\boldsymbol{z})$ values. To identify the optimal trade-off solution from the Pareto front, the knee point method was applied (Yu et al. 2022), where the trade-off model (red circles) gives 2.70 and 0.34 in Model 1 and 2.43 and 0.44 in Model 2 for data misfit $F_1(\boldsymbol{z})$ and model constraint $F_2(\boldsymbol{z})$, respectively.

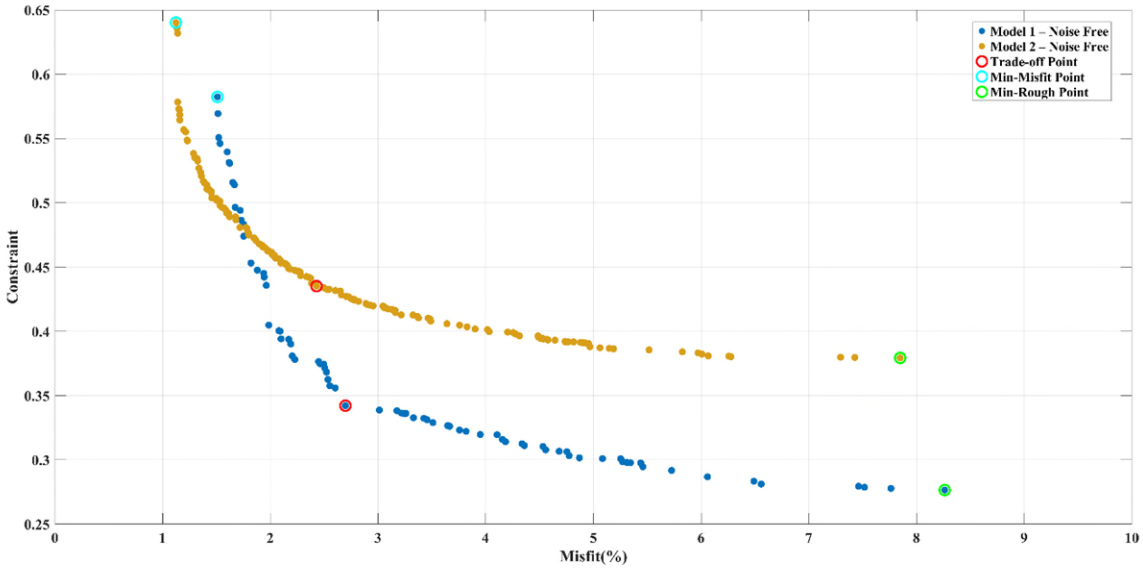


Figure 5 Pareto front (PF) obtained from noise-free gravity data inversion of synthetic models namely Model 1 and Model 2, illustrating the trade-off between data misfit $F_1(\boldsymbol{z})$ and model constraint $F_2(\boldsymbol{z})$. Red circle indicates the knee point solution representing the optimal trade-off between the two competing objectives.

Pareto-optimal solutions (POS), which are multiple sets of solutions for multi-objective problems correlated with the Pareto-optimal front (POF), are collectively considered optimal, because no single solution is superior in meeting all objectives (Deb 2011). The accurate estimation of the Pareto-optimal solution set in multi-objective problems is crucial because it enables the calculation of the uncertainty associated with each estimated model parameter. Consequently, POS can be directly utilized as the inversion solution, and the uncertainty of model parameters can be determined through the standard deviation of POS (Dal Moro and Pipan 2007; Dal Moro 2008). In addition to uncertainty quantification, statistical descriptors of the solution ensemble including the mean or median as measures of central tendency, and the interquartile range or standard deviation as measures of dispersion, can be employed to derive a representative inversion solution and to convey the associated model parameter variability in a statistically rigorous manner.

Figure 6 and Figure 7 present a comparison between the observed and calculated gravity anomaly data (upper panel) and the subsurface basement depth models revealed by POS (lower panel) for Model 1 and Model 2 synthetic models, respectively. Model uncertainty is quantified through the interquartile range (Iqr) of the POS, while the median of the subset of POS corresponding to a data misfit $\leq$ 10% identified from the PF is adopted as the representative inversion solution. The POS ensemble and its associated statistical descriptors demonstrate close agreement with the true synthetic model, confirming the accuracy and reliability of the proposed multi-objective inversion approach under noise-free conditions.

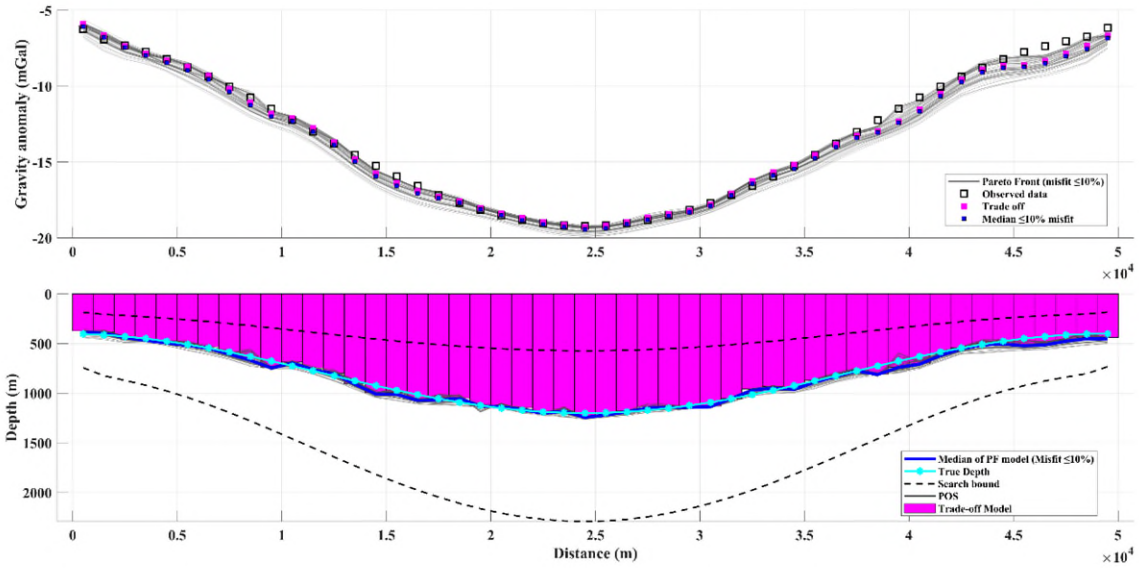


Figure 6 Basement depth solutions recovered from synthetic gravity dataset of Model 1 under the noise-free case. Upper panel: Comparison between the original observed and calculated residual gravity anomalies. Lower panel: Boundaries model and POS with the true model.

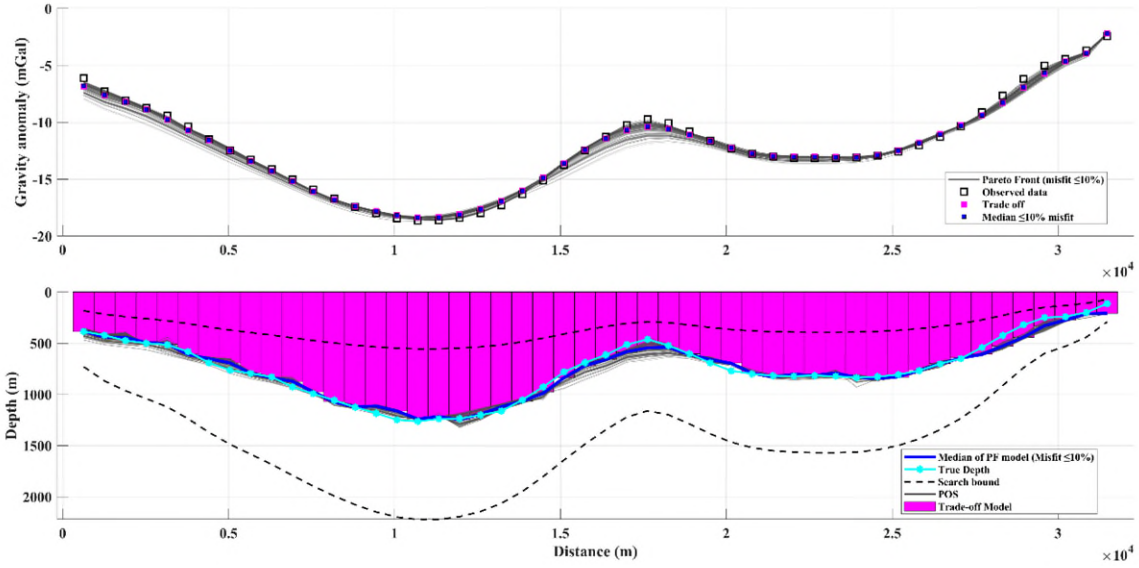


Figure 7 Basement depth solutions recovered from synthetic gravity dataset of Model 2 under the noise-free case. Upper panel: Comparison between the original observed and calculated residual gravity anomalies. Lower panel: Boundaries model and POS with the true model.

4.2 Noise-Added

The noise-added gravity datasets were inverted under identical algorithmic conditions as those applied to the noise-free synthetic data, with all AMALGAM parameters remaining unchanged, thereby ensuring a consistent and directly comparable evaluation of algorithm performance. The results were subsequently compared with the original model. Table 1 shows that the statistics of both objectives (misfit and constraint) for the noise-added case are higher than those for the noise-free case. This outcome is physically consistent with the effect of additive noise, which distorts the misfit function topography and consequently broadens the range of admissible solutions within the Pareto front (Fernández-Martínez et al. 2014b). Nevertheless, the standard deviation of both objective function values is also low, implying that there is no issue with the distribution of the objective function values. Figure 8 shows the PF resulting from the inversion of the noisy gravity data for both models. The trade-off solutions show that Model 1 is characterized by a misfit of 6.17 and a constraint model of 0.76, while the corresponding values for Model 2 are 7.86 and 0.64, respectively.

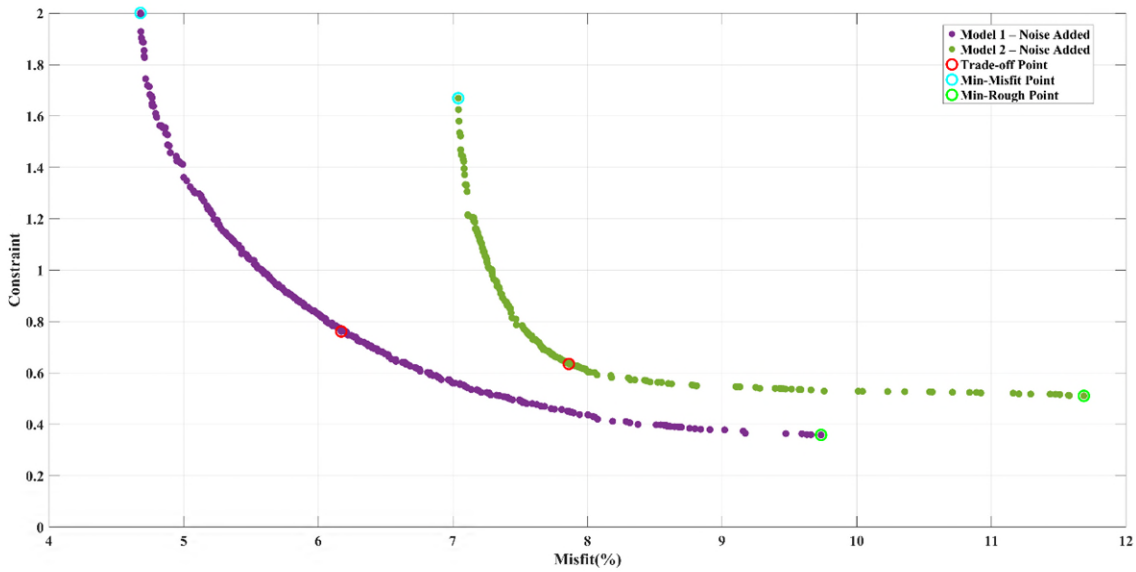


Figure 8 Pareto front (PF) obtained from noise-added gravity data inversion of synthetic models namely Model 1 and Model 2, illustrating the trade-off between data misfit $F_1(\boldsymbol{z})$ and model constraint $F_2(\boldsymbol{z})$. Red circle indicates the knee point solution representing the optimal trade-off between the two competing objectives.

Figure 9 and Figure 10 present the inversion results for the noise-added synthetic gravity datasets for Model 1 and Model 2, respectively, illustrating POS, trade-off model, median of POS with misfit $\leq 10\%$, and Iqr model or model uncertainty. The inversion results demonstrate that the multi-objective AMALGAM approach maintains stable and reliable performance in the presence of random noise, successfully recovering basement depth geometries that are in close agreement with the true synthetic models despite the degraded data quality.

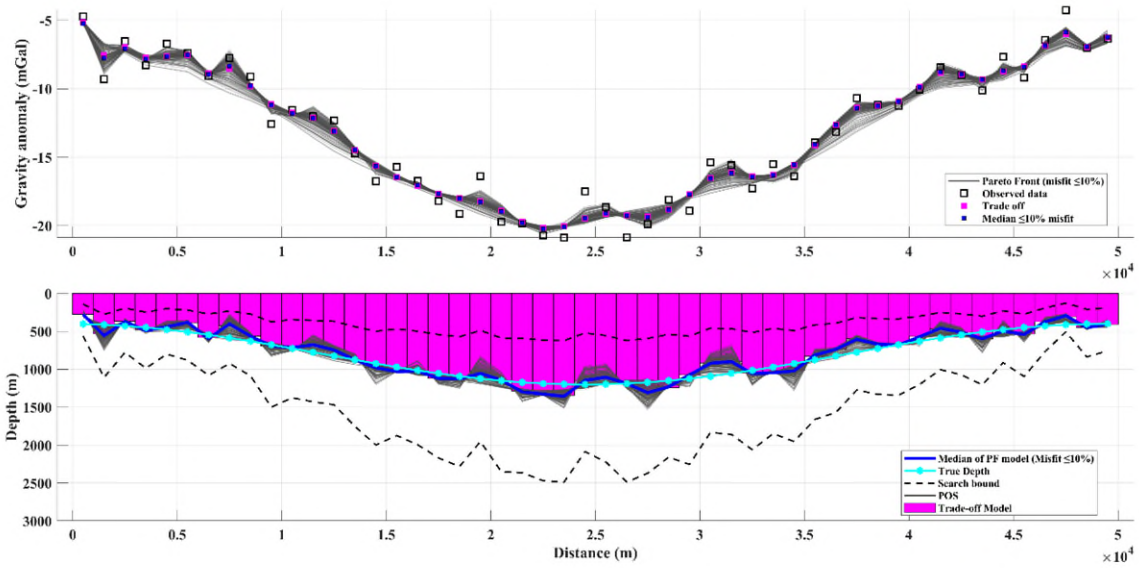


Figure 9 Inversion results for the 10% noise-added gravity data of Model 1 using the multi-objective AMALGAM approach. Upper panel: Comparison between the noise-added synthetic gravity data and the calculated gravity anomaly reproduced by the inversion models. Lower panel: True synthetic basement depth model overlain by the Pareto-optimal solution ensemble (POS) and prescribed search space boundaries.

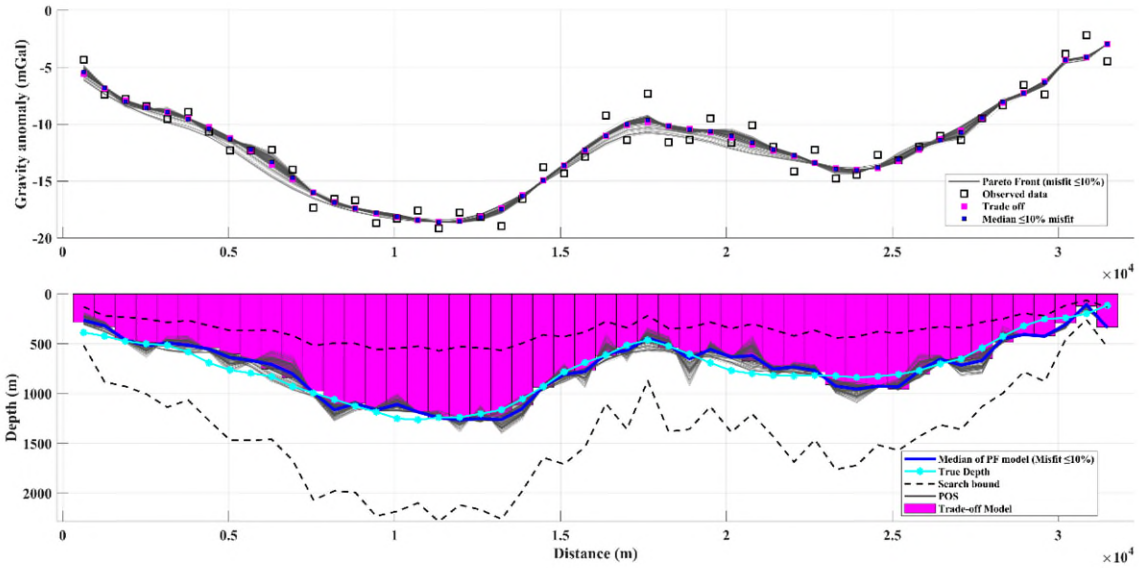


Figure 10 Inversion results for the 10% noise-added gravity data of Model 2 using the multi-objective AMALGAM approach. Upper panel: Comparison between the noise-added synthetic gravity data and the calculated gravity anomaly reproduced by the inversion models. Lower panel: True synthetic basement depth model overlain by the Pareto-optimal solution ensemble (POS) and prescribed search space boundaries.

5. Field Studies

To further validate the proposed multi-objective inversion framework under real-world conditions, gravity anomaly data from two well-documented sedimentary basin (the Büyük Menderes Graben in western Türkiye and the Moghan sedimentary basin in northwest Iran) were inverted using the AMALGAM algorithm with identical parameter settings as those employed in the synthetic studies, namely a population size of 500 and a maximum of 100 iterations. Given that each iteration requires the execution of 500 forward modelling and objective function evaluations, the complete inversion process for each field dataset necessitates a total of 50,000 forward

433 modelling computations (500×100), encompassing both the initial population evaluations and all
434 subsequent iterative updates.

435 **5.1 Büyük Menderes Graben**

436 The Büyük Menderes Graben (BMG) is one of the major tectonic elements in western
437 Türkiye. Its formation is attributed to the complex interaction between the northward-moving
438 African, Arabian, Indian plates, and the Eurasian plate within an extensional tectonic regime
439 (Bozkurt 2001). Crustal extension driven by the subduction of the African plate along the Aegean
440 and Cyprus Arcs has produced a system of horsts and grabens across the region (Hancock and
441 Barka 1987). Among these tectonic structures, the Büyük Menderes Graben (BMG) (Figure 11)
442 represents a major graben system developed along the southern and northern flanks of the Central
443 Menderes Massif and is filled with Neogene–Quaternary continental sediments deposited in
444 lacustrine, alluvial, and fluvial environments (Çifçi et al. 2011).

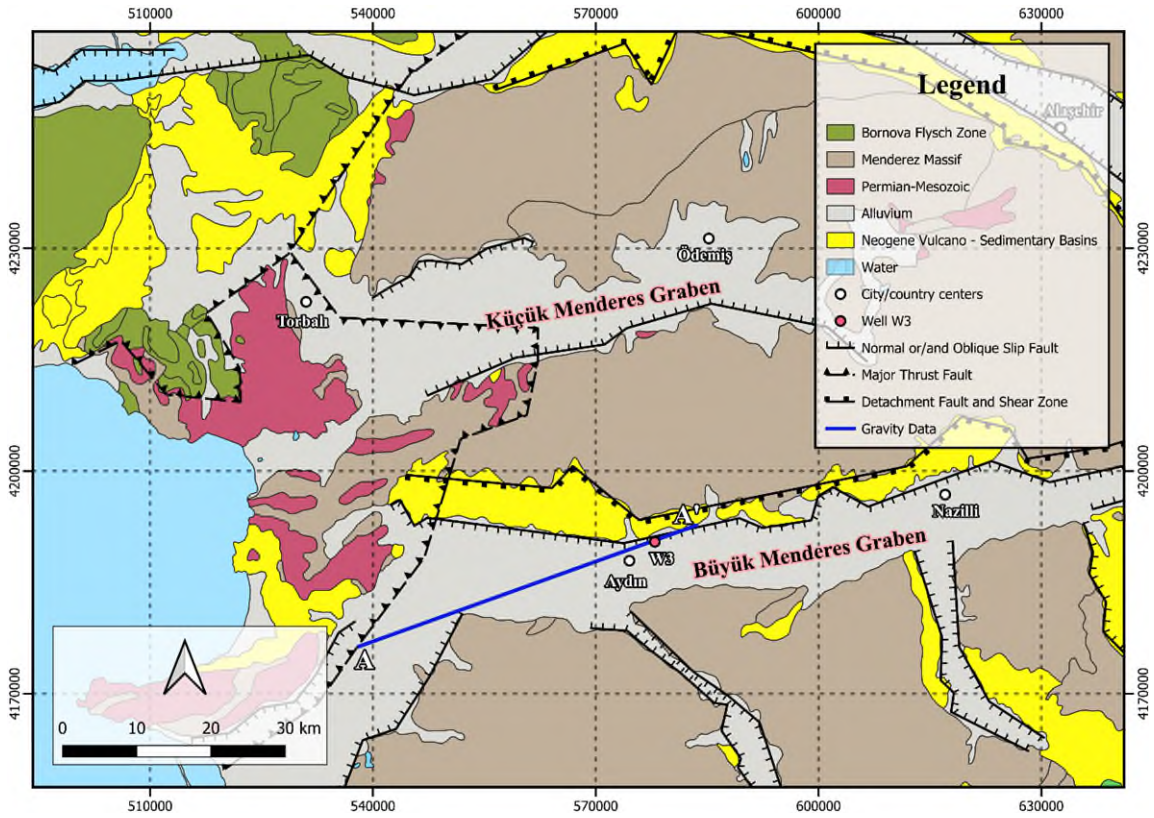
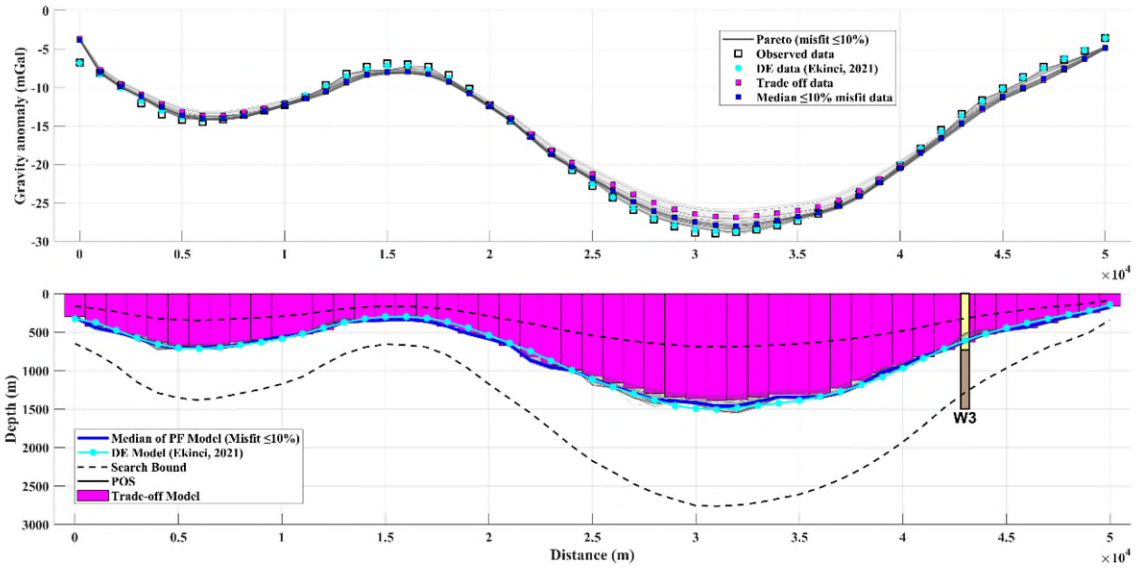


Figure 11 Geological map of the Büyük Menderes Graben (BMG) showing the locations of measured gravity data acquisition profile (line AA') and available borehole data (W3) (modified after (Ekinci et al. 2021).

The BMG region is widely recognized as one of the most significant geothermal areas in Türkiye, a characteristic directly attributable to the area's intense regional tectonic and volcanic activity (Pamukçu et al. 2019). Previous investigation employing gravity and seismic methods have been conducted to estimate sedimentary thickness and the depth to metamorphic basement rocks within the graben (Çifçi et al. 2011; Ekinci et al. 2021). In the present study, the local gravity anomaly profile (Figure 12, upper panel) was inverted using the multi-objective AMALGAM framework to determine the basement depth geometry of the BMG and its associated model uncertainty. The gravity profile spans approximately 50 km, comprising 51 equally spaced observation points at intervals of 1 km. Accordingly, the horizontal width of each rectangular

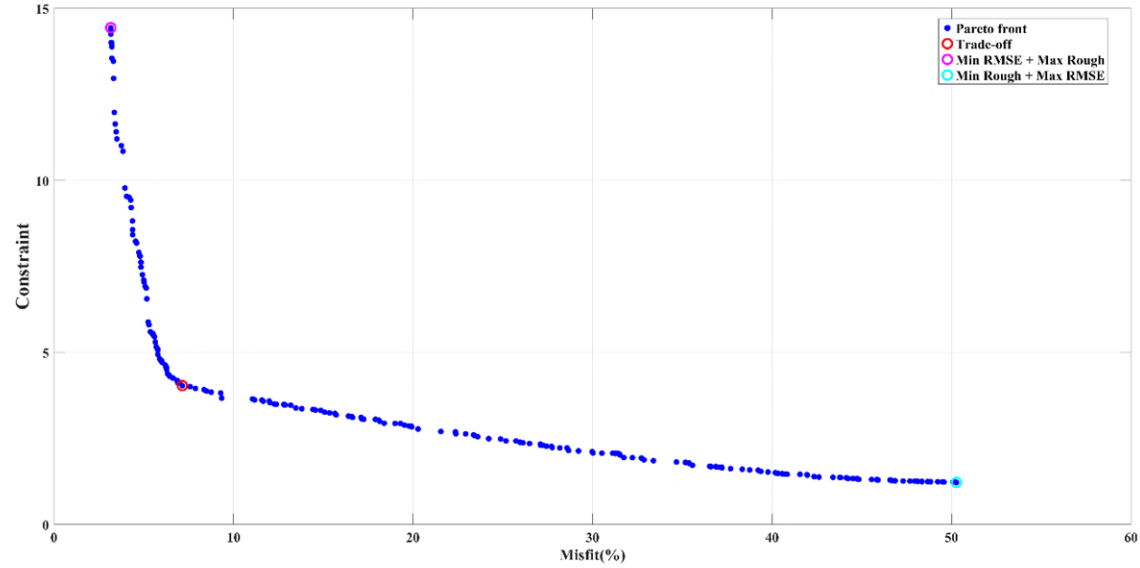
458 prism in the inversion model is set to 1 km. The density contrast between the Neogene-Quaternary
459 sedimentary fill and the pre-Neogene metamorphic basement in the study area is adopted as 500
460 kg/m³ (Sari and Şalk 2006), and this value is held constant throughout the multi-objective inversion
461 procedure.

462 Figure 13 shows the PF obtained from the inversion of the BMG gravity data, spanning a
463 data misfit range of 3.16–50.27 and a model constraint range of 1.23–14.44. The knee point trade-
464 off solution yields a data misfit of 7.15 and a model constraint value of 4.039. The lower panel of
465 Figure 12 illustrates the POS in comparison with the basement depth solution obtained
466 independently using Differential Evolution (DE) inversion (Ekinci et al. 2021) and the available
467 lithological borehole log data (Akkuş et al. 2005). The POS and its associated uncertainty model
468 demonstrate satisfactory agreement with both the DE-derived solution and the lithological
469 borehole constraints, as evidenced in Figure 12. At the borehole location, the POS yields basement
470 estimates within the range [0.51, 0.65] km, with a median value and uncertainty of 0.61 ± 0.06 km.
471 The trade-off solution and the borehole-constrained depth estimate yield value of 0.63 and 0.61
472 km, respectively, while the DE inversion solution produces a depth of 0.61 km. These results
473 collectively confirm that the multi-objective inversion approach yields basement depth estimates
474 that are in close agreement with both the independent single-objective DE solution and the
475 available drilling data, thereby validating the reliability of the proposed framework for field
476 applications.
477



478

479 Figure 12 Inversion result of the BMG gravity data. Upper panel: Comparison between the
480 observed gravity anomaly and calculated gravity response revealed by the AMALGAM
481 inversion models. Lower panel: Basement depth solutions derived from the POS, DE, and
482 lithological borehole log (W3).



483

484 Figure 13. PF obtained from the multi-objective inversion of the observed gravity data from the
485 BMG, illustrating the trade-off between data misfit and model constraint objectives.

486 Table 2 shows the maximum basement depth comparison between this study and previous
487 studies. According to the aforementioned table, the close correspondence between the multi-

objective inversion results and those obtained independently through the DE algorithm (Ekinci et al. 2021, 2023), DL approach (Roy et al. 2025), and MJAYA algorithm (Lestari et al. 2026) further corroborates the validity, consistency, and practical applicability of the proposed AMALGAM-based multi-objective inversion framework for field-scale basement depth estimation.

Table 2 Comparison of maximum basement depth estimates for the BMG obtained using the proposed multi-objective AMALGAM inversion approach and alternative methods reported in the literature.

Inversion Methods	Forward modeling	Maximum depth of the basement (km)
DE (Ekinci et al. 2021)	2D	1.51
DE (Ekinci et al. 2023)	3D	1.75
Deep Learning (Roy et al. 2025)	2D	1.49
MJAYA (Lestari et al. 2026)	2D	1.52 ± 0.02
Ranges of the AMALGAM	2D	[1.33,1.53]
Trade-off		1.39
Median and uncertainty		1.46 ± 0.07

5.2 Moghan Sedimentary Basin

Following successful validation of the proposed multi-objective inversion framework on the BMG gravity data, the AMALGAM algorithm was subsequently applied to gravity data acquired over the Moghan sedimentary basin in northwestern Iran. The Moghan sedimentary basin is located to the west of the Caspian Sea bounded by the Republic of Azerbaijan to the north and west, and the Qaradagh Mountains to the south (Joolaei et al. 2022). The basin's tectonic evolution is governed by the ongoing collision between the Arabian and Eurasian plates, an active geodynamic process that has driven orogenic deformation and produced a complex system of folds and faults spanning from the Neogene to the Quaternary periods.

The Moghan region has attracted considerable attention in geophysical studies and resource exploration owing to several strategically important factors, including its geographical proximity to the Baku oil field, the presence of substantial sedimentary deposits, the occurence of numerous hot springs, and ongoing hydrocarbon exploration activities (Jafarzadeh et al. 2014). Previous gravimetric studies of the Moghan region have identified Eocene volcanic materials, particularly basalt flows, as the principal basement rock. These volcanic rocks exhibit a sufficient density contrast with respect to the overlying sedimentary layers, rendering gravity data an effective tool for imaging the basement relief geometry (Nejati et al., 2010).

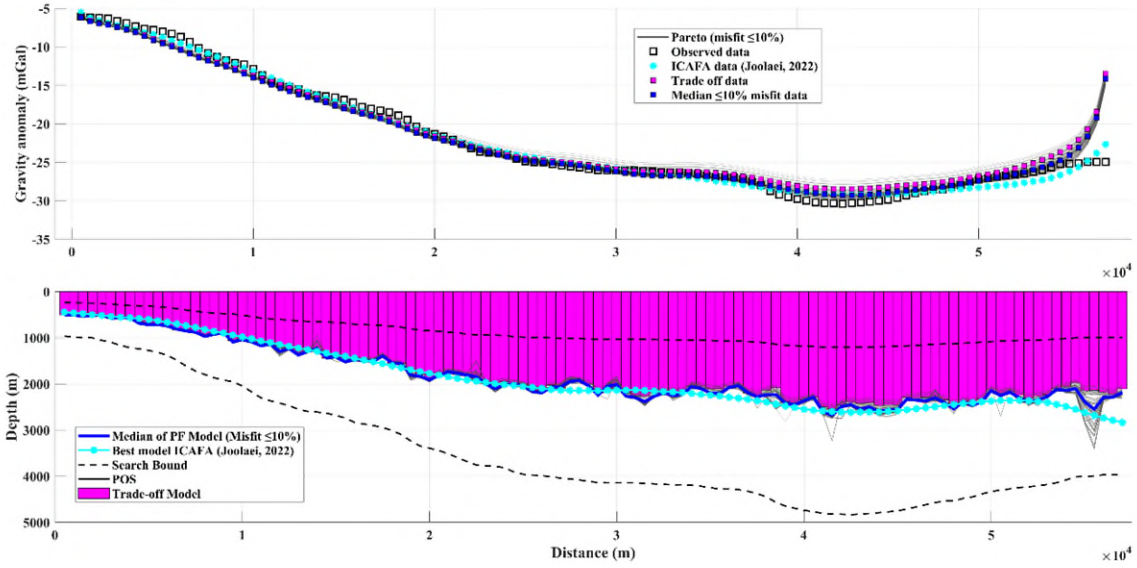


Figure 14 Basement depth of the Moghan sedimentary basin, northwestern Iran, revealed from gravity data inversion using the multi-objective AMALGAM approach. Upper panel: Comparison between the observed and calculated gravity anomaly data. Lower panel: 2D basement depth profile derived from the PF, trade-off model, and median of PF with misfit $\leq 10\%$ compared with combination between Imperialist Competitive Algorithm (ICA) and Firefly Algorithm (FA) (ICAFA) (Joolaei et al., 2022).

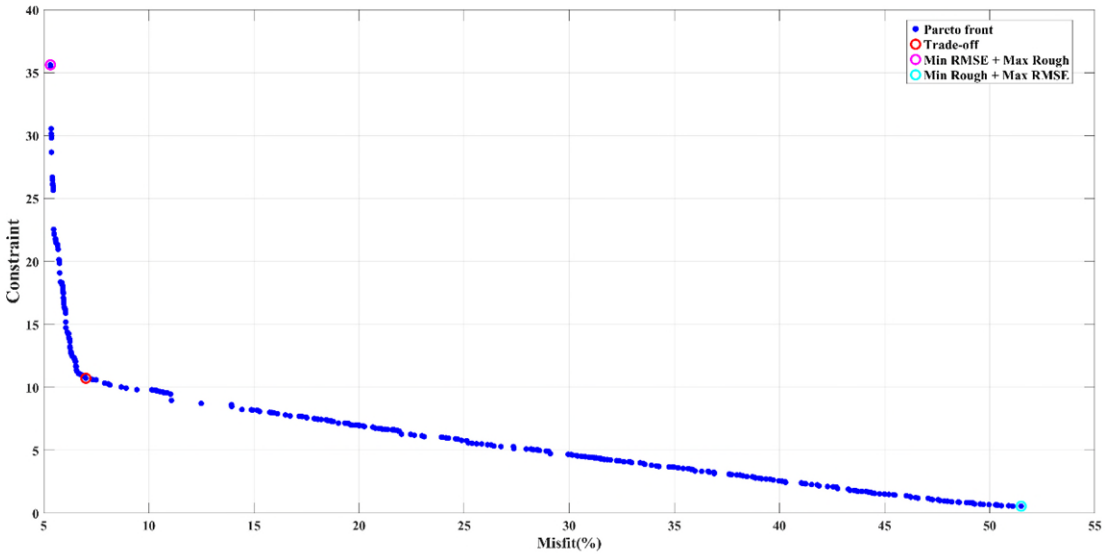


Figure 15 Pareto front (PF) obtained from the multi-objective inversion of gravity data acquired over the Moghan sedimentary basin, northwestern Iran.

The residual gravity anomaly profile the Moghan area was digitized from previously published data (Joolaei et al. 2022), as shown in the upper panel of Figure 14. The gravity data were inverted using the multi-objective AMALGAM framework, employing a model discretization of 120 rectangular prisms with a uniform horizontal width of 500 m and a density contrast of -300 kg/m^3 (Joolaei et al. 2022). The Pareto front (PF) resulting from the AMALGAM inversion is presented in Figure 15, encompassing a data misfit ranges of [5.32, 51.50] and a model constraint ranges of [0.56,35.63]. The trade-off solution yields a data misfit of 7.00 and a model constrain of 10.72. The inversion results for the Moghan gravity data are presented in the lower panel of Figure 14. The result indicates that the basement model for the multi-objective (POF, trade-off model, and median) is in close agreement with the optimal model of combination of Imperialist Competitive Algorithm (ICA) and Firefly Algorithm (ICAFA), except on the right edge. The condition may be caused by the end effect.

6. Conclusions

This study presents a multi-objective optimization framework based on the AMALGAM algorithm for 2D gravity data inversion and model appraisal of basement relief in sedimentary basins, in which the subsurface is parameterized as an aggregate of rectangular prisms. The principal objective of the proposed approach is to simultaneously minimize two competing objective functions (the data misfit term and the model smoothness constraint) without requiring post-inversion smoothing or spectral filtering of model parameters, gradient information, or the subjective prescription of a regularization parameter. By treating these two objectives as independent and competing functions, the multi-objective framework generates an ensemble of Pareto-optimal solutions that collectively represent a diverse range of trade-offs between data fitness and model complexity, thereby providing a rigorous and quantitative basis for model uncertainty assessment. The robustness and reliability of the proposed inversion framework were first systematically evaluated using two synthetic basement depth models under both noise-free and noise-added conditions. The results demonstrate that the Pareto-optimal solution ensemble yields basement depth estimates in close agreement with the true synthetic models in both scenarios, confirming the algorithm's stability and accuracy across varying levels of data quality and structural complexity. The proposed approach was subsequently applied to field gravity datasets acquired over two well-documented sedimentary basins: the Büyük Menderes Graben in western Türkiye and the Moghan sedimentary basin in northwestern Iran. In both field applications, the recovered basement depth models and their associated uncertainty estimates demonstrate strong consistency with results obtained by independent inversion algorithms and available borehole lithological data, further validating the practical applicability and geological reliability of the proposed framework. The findings of this study collectively establish the

AMALGAM-based multi-objective inversion approach as a robust, accurate, and computationally efficient method for basement depth estimation and subsurface imaging in geophysical exploration of sedimentary basins.

Acknowledgments

This research is funded by the Indonesian Endowment Fund for Education (LPDP) on behalf of the Indonesian Ministry of Higher Education, Science and Technology and managed under the EQUITY Program (Contract No 4299/B3/DT.03.08/2025 & No 3029/PKS/ITS/2025). AMALGAM, which was developed by Jasper A. Vrugt, can be accessed in the https://github.com/jaspervrugt/AMALGAM. BMG gravity data was shared by Prof. Ekinci, while the Moghan gravity data was digitized from https://doi.org/10.1007/s11600-021-00597-3.

References

Akca İ, Günther T, Müller-Petke M, et al (2014) Joint parameter estimation from magnetic resonance and vertical electric soundings using a multi-objective genetic algorithm. Geophys Prospect 62:364–376. https://doi.org/10.1111/1365-2478.12082

Akkuş İ, Akıllı H, Ceyhan S, et al (2005) Inventory of Turkey Geothermal Sources. Inventory Ser-201

An Y, Fan T, Li P, et al (2025) Archived multi-objective simulated annealing transient electromagnetic inversion. Sci Rep 15:41769. https://doi.org/10.1038/s41598-025-25699-6

Barbosa VCF, Silva JBC, Medeiros WE (1999) Gravity inversion of a discontinuous relief stabilized by weighted smoothness constraints on depth. Geophysics 64:1429–1437. https://doi.org/10.1190/1.1444647

Barbosa VCF, Silva JBC, Medeiros WE (1997) Gravity inversion of basement relief using approximate equality constraints on depths. Geophysics 62:1745–1757. https://doi.org/10.1190/1.1444275

Bijani R, Lelièvre PG, Ponte-Neto CF, Farquharson CG (2017) Physical-property-, lithology- and surface-geometry-based joint inversion using Pareto Multi-Objective Global Optimization. Geophys J Int 209:730–748. https://doi.org/10.1093/gji/ggx046

Biswas A, Acharya T (2016) A very fast simulated annealing method for inversion of magnetic anomaly over semi-infinite vertical rod-type structure. Model Earth Syst Environ 2:1–10. https://doi.org/10.1007/s40808-016-0256-x

Bohidar RN, Sullivan JP, Hermance JF (2001) Delineating Depth to Bedrock Beneath Shallow Unconfined Aquifers: A Gravity Transect Across the Palmer River Basin. Groundwater 39:729–736. https://doi.org/10.1111/j.1745-6584.2001.tb02363.x

Bott MHP (1960) The use of Rapid Digital Computing Methods for Direct Gravity Interpretation of Sedimentary Basins. Geophys J R Astron Soc 3:63–67. https://doi.org/10.1111/j.1365-246X.1960.tb00065.x

Bozkurt E (2001) Neotectonics of Turkey – a synthesis. Geodin Acta 14:3–30. https://doi.org/10.1016/S0985-3111(01)01066-X

Çifçi G, Pamukçu O, Çoruh C, et al (2011) Shallow and Deep Structure of a Supradetachment Basin Based on Geological, Conventional Deep Seismic Reflection Sections and Gravity Data in the Buyuk Menderes Graben, Western Anatolia. Surv Geophys 32:271–290. https://doi.org/10.1007/s10712-010-9109-8

Dal Moro G (2008) *V*S and *V*P vertical profiling via joint inversion of Rayleigh waves and refraction travel times by means of bi-objective evolutionary algorithm. J Appl Geophys 66:15–24. https://doi.org/10.1016/j.jappgeo.2008.08.002

Dal Moro G, Pipan M (2007) Joint inversion of surface wave dispersion curves and reflection travel times via multi-objective evolutionary algorithms. J Appl Geophys 61:56–81. https://doi.org/10.1016/j.jappgeo.2006.04.001

Deb K (2011) Multi-objective Optimisation Using Evolutionary Algorithms: An Introduction. In: Wang L, Ng AHC, Deb K (eds) Multi-objective Evolutionary Optimisation for Product Design and Manufacturing. Springer, London, pp 3–34

Deb K, Agrawal RB (1995) Simulated Binary Crossover for Continuous Search Space. Complex Syst 9:115–148

Deb K, Anand A, Joshi D (2002a) A Computationally Efficient Evolutionary Algorithm for Real-Parameter Optimization. Evol Comput 10:371–395. https://doi.org/10.1162/106365602760972767

Deb K, Pratap A, Agarwal S, Meyarivan T (2002b) A fast and elitist multiobjective genetic algorithm: NSGA-II. IEEE Trans Evol Comput 6:182–197. https://doi.org/10.1109/4235.996017

Ekinci YL, Balkaya Ç, Göktürkler G, Ai H (2023) 3-D gravity inversion for the basement relief reconstruction through modified success-history-based adaptive differential evolution. Geophys J Int 235:377–400. https://doi.org/10.1093/gji/ggad222

Ekinci YL, Balkaya Ç, Göktürkler G, Özyalın Ş (2021) Gravity data inversion for the basement relief delineation through global optimization: a case study from the Aegean Graben System, western Anatolia, Turkey. 224:

Essa KS, Diab ZE, Gomaa OA, Elhussein M (2025a) Enhanced self-potential inversion using a hybrid Second Horizontal Gradient and Bat Algorithm–SHGBA-framework for geothermal reservoir characterization. Sci Rep 15:40407. https://doi.org/10.1038/s41598-025-17101-2

Essa KS, Gomaa OA, Elhussein M, et al (2025b) A prosperous and thorough analysis of gravity profiles for resources exploration utilizing the metaheuristic Bat Algorithm. Sci Rep 15:5000. https://doi.org/10.1038/s41598-025-88350-4

Fernández Martínez JL, Fernández Muñiz MZ, Tompkins MJ (2012) On the topography of the cost functional in linear and nonlinear inverse problems. Geophysics 77:W1–W15. https://doi.org/10.1190/geo2011-0341.1

Fernández-Martínez JL, Fernández-Muñiz Z, Pallero JLG, Pedruelo-González LM (2013) From Bayes to Tarantola: New insights to understand uncertainty in inverse problems. J Appl Geophys 98:62–72. https://doi.org/10.1016/j.jappgeo.2013.07.005

Fernández-Martínez JL, Pallero JLG, Fernández-Muñiz Z, Pedruelo-González LM (2014a) The effect of noise and Tikhonov's regularization in inverse problems. Part II: The nonlinear case. J Appl Geophys 108:186–193. https://doi.org/10.1016/j.jappgeo.2014.05.005

Fernández-Martínez JL, Pallero JLG, Fernández-Muñiz Z, Pedruelo-González LM (2014b) The effect of noise and Tikhonov's regularization in inverse problems. Part I: The linear case. J Appl Geophys 108:176–185. https://doi.org/10.1016/j.jappgeo.2014.05.006

Haario H, Saksman E, Tamminen J (2001) An adaptive Metropolis algorithm. Bernoulli 7:223–242

Hancock PL, Barka AA (1987) Kinematic indicators on active normal faults in Western Turkey. J Struct Geol 9:573–584. https://doi.org/10.1016/0191-8141(87)90142-8

Harding TP, Tuminas AC (1989) Structural Interpretation of Hydrocarbon Traps Sealed by Basement Normal Block Faults at Stable Flank of Foredeep Basins and at Rift Basins1. AAPG Bull 73:812–840. https://doi.org/10.1306/44B4A276-170A-11D7-8645000102C1865D

Horikawa T, Kusumoto S (2025) Delineation of multilayered structure based on constrained gravity inversion for geothermal resource development. Earth Planets Space 78:1. https://doi.org/10.1186/s40623-025-02328-0

Huisman JA, Rings J, Vrugt JA, et al (2010) Hydraulic properties of a model dike from coupled Bayesian and multi-criteria hydrogeophysical inversion. J Hydrol 380:62–73. https://doi.org/10.1016/j.jhydrol.2009.10.023

Jafarzadeh M, Harami RM, Friis H, et al (2014) Provenance of the Oligocene–Miocene Zivah Formation, NW Iran, assessed using heavy mineral assemblage and detrital clinopyroxene and detrital apatite analyses. J Afr Earth Sci 89:56–71. https://doi.org/10.1016/j.jafrearsci.2013.10.005

Jamasb A, Motavalli-Anbaran S-H, Ghasemi K (2019) A Novel Hybrid Algorithm of Particle Swarm Optimization and Evolution Strategies for Geophysical Non-linear Inverse Problems. Pure Appl Geophys 176:1601–1613. https://doi.org/10.1007/s00024-018-2059-7

Jamasb A, Motavalli-Anbaran S-H, Zeyen H (2017) Non-linear stochastic inversion of gravity data via quantum-behaved particle swarm optimisation: application to Eurasia–Arabia collision zone (Zagros, Iran). Geophys Prospect 65:274–294. https://doi.org/10.1111/1365-2478.12558

Joolaei A, Arab-Amiri A, Nejati A (2022) Gravity inversion of basement relief using imperialist competitive algorithm with hybrid techniques. Acta Geophys 70:2629–2646. https://doi.org/10.1007/s11600-021-00597-3

Kennedy J, Eberhart R (1995) Particle swarm optimization. In: Proceedings of ICNN'95 - International Conference on Neural Networks. pp 1942–1948 vol.4

Lestari S, Sungkono S, Saifuddin S, et al (2026) Simultaneous estimation of hyperparameters and basement depth in gravity data inversion using the JAYA algorithm. Artif Intell Geosci 7:100245. https://doi.org/10.1016/j.aiig.2026.100245

Lima WA, Martins CM, Silva JBC, Barbosa VCF (2011) Total variation regularization for depth-to-basement estimate: Part 2 — Physicogeologic meaning and comparisons with previous inversion methods. Geophysics 76:I13–I20. https://doi.org/10.1190/1.3524547

Lyu Q, Wang W, Jiang Q, et al (2023) Basement Reservoirs in China: Distribution and Factors Controlling Hydrocarbon Accumulation. Minerals 13:1052. https://doi.org/10.3390/min13081052

Martins CM, Lima WA, Barbosa VCF, Silva JBC (2011) Total variation regularization for depth-to-basement estimate: Part 1 — Mathematical details and applications. Geophysics 76:I1–I12. https://doi.org/10.1190/1.3524286

Onajite E (2013) Seismic Data Analysis Techniques in Hydrocarbon Exploration. Elsevier

Pallero JLG, Fernández-Martínez JL, Bonvalot S, Fudym O (2015) Gravity inversion and uncertainty assessment of basement relief via Particle Swarm Optimization. J Appl Geophys 116:180–191. https://doi.org/10.1016/j.jappgeo.2015.03.008

Pallero JLG, Fernández-Martínez JL, Bonvalot S, Fudym O (2017) 3D gravity inversion and uncertainty assessment of basement relief via Particle Swarm Optimization. J Appl Geophys 139:338–350. https://doi.org/10.1016/j.jappgeo.2017.02.004

693 Pallero JLG, Fernández-Martínez JL, Fernández-Muñiz Z, et al (2021) GravPSO2D: A Matlab
694 package for 2D gravity inversion in sedimentary basins using the Particle Swarm
695 Optimization algorithm. Comput Geosci 146:104653.
696 https://doi.org/10.1016/j.cageo.2020.104653

697 Pamukçu O, Gönenç T, Çırmık A, et al (2019) The Geothermal Potential of Büyük Menderes
698 Graben Obtained by Combined 2.5-D Normalized Full Gradient Results. Pure Appl
699 Geophys 176:5003–5026. https://doi.org/10.1007/s00024-019-02227-y

700 Panthi J, Johnson CD, Pradhanang SM, et al (2023) Delineating bedrock topography with
701 geophysical techniques: An implication for groundwater mapping. CATENA 230:107258.
702 https://doi.org/10.1016/j.catena.2023.107258

703 Peng W, Cheng T, Wang S, et al (2025) Basement depth estimation of the Red Sea basin from
704 gravity data and drilling data. J Geophys Eng 22:963–970.
705 https://doi.org/10.1093/jge/gxaf046

706 Ramadhan AN, Sungkono, Rizaq AM, et al (2024) Multi-anomalies self-potential inversion using
707 enhanced Runge–Kutta optimization. J Earth Syst Sci 133:14.
708 https://doi.org/10.1007/s12040-023-02225-8

709 Roy A, Dubey CP, Prasad M (2021a) Gravity inversion of basement relief using Particle Swarm
710 Optimization by automated parameter selection of Fourier coefficients. Comput Geosci
711 156:104875. https://doi.org/10.1016/j.cageo.2021.104875

712 Roy A, Dubey CP, Prasad M (2021b) Gravity inversion for heterogeneous sedimentary basin with
713 b-spline polynomial approximation using differential evolution algorithm. Geophysics
714 86:F35–F47. https://doi.org/10.1190/geo2019-0779.1

715 Roy A, Ekinci YL, Balkaya Ç, Ai H (2025) Deep learning-based inversion with discrete cosine
716 transform discretization for two-dimensional basement relief imaging of sedimentary
717 basins from observed gravity anomalies. Geophys Prospect 73:113–129.
718 https://doi.org/10.1111/1365-2478.13647

719 Saifuddin S, Sungkono S, Rochman JPGN (2025) Geomagnetic Data Inversion Using Modified
720 JAYA Algorithm and Application to Mineral Exploration. Arab J Sci Eng.
721 https://doi.org/10.1007/s13369-025-10724-7

722 Santos DF, Silva JBC, Martins CM, et al (2015) Efficient gravity inversion of discontinuous
723 basement relief. Geophysics 80:G95–G106. https://doi.org/10.1190/geo2014-0513.1

724 Sari C, Şalk M (2006) Sediment thicknesses of the western Anatolia graben structures determined
725 by 2D and 3D analysis using gravity data. J Asian Earth Sci 26:39–48.
726 https://doi.org/10.1016/j.jseaes.2004.09.011

727 Silva JBC, Santos DF, Gomes KP (2014) Fast gravity inversion of basement relief. Geophysics
728 79:G79–G91. https://doi.org/10.1190/geo2014-0024.1

729 Storn R, Price K (1997) Differential Evolution – A Simple and Efficient Heuristic for global
730 Optimization over Continuous Spaces. J Glob Optim 11:341–359.
731 https://doi.org/10.1023/A:1008202821328

732 Sungkono (2020) An efficient global optimization method for self-potential data inversion using
733 micro-differential evolution. J Earth Syst Sci 129:178. https://doi.org/10.1007/s12040-
734 020-01430-z

735 Sungkono S, Rochman JPGN, Saifuddin, et al (2025) Enhanced generalized normal distribution
736 optimization for interpreting magnetic data caused by subsurface mineral deposits. Earth
737 Sci Inform 18:451. https://doi.org/10.1007/s12145-025-01948-0

738 Telford WM, Geldart LP, Sheriff RE (1990) Applied Geophysics. Cambridge University Press

739 Vrugt JA (2015) Multi-criteria optimization using the AMALGAM software package: Theory,
740 concepts, and MATLAB implementation

741 Vrugt JA, Gupta HV, Bastidas LA, et al (2003) Effective and efficient algorithm for multiobjective
742 optimization of hydrologic models. Water Resour Res 39:.
743 https://doi.org/10.1029/2002WR001746

744 Vrugt JA, Robinson BA (2007) Improved evolutionary optimization from genetically adaptive
745 multimethod search. Proc Natl Acad Sci 104:708–711.
746 https://doi.org/10.1073/pnas.0610471104

747 Vrugt JA, Robinson BA, Hyman JM (2009) Self-Adaptive Multimethod Search for Global
748 Optimization in Real-Parameter Spaces. IEEE Trans Evol Comput 13:243–259.
749 https://doi.org/10.1109/TEVC.2008.924428

750 Warnana DD, Sungkono S, S. Essa K (2025) Efficient and Robust Estimation of Various Ore and
751 Mineral Model Parameters from Residual Gravity Anomalies Using the Dual Classification
752 Learning Rao Algorithm. Arab J Sci Eng 50:14931–14960.
753 https://doi.org/10.1007/s13369-024-09774-0

754 Weissmann GS, Hartley AJ, Scuderi LA, et al (2015) Fluvial geomorphic elements in modern
755 sedimentary basins and their potential preservation in the rock record: A review.
756 Geomorphology 250:187–219. https://doi.org/10.1016/j.geomorph.2015.09.005

757 Wolpert DH, Macready WG (1997) No free lunch theorems for optimization. IEEE Trans Evol
758 Comput 1:67–82. https://doi.org/10.1109/4235.585893

759 Xing Z, Mazzotti A (2019) Two-grid full-waveform Rayleigh-wave inversion via a genetic
760 algorithm — Part 2: Application to two actual data sets. Geophysics 84:R815–R825.
761 https://doi.org/10.1190/geo2018-0800.1

762 Xiong J, Zhang T (2015) Multiobjective particle swarm inversion algorithm for two-dimensional
763 magnetic data. Appl Geophys 12:127–136. https://doi.org/10.1007/s11770-015-0486-0

Yu X, Duan Y, Luo W (2022) A knee-guided algorithm to solve multi-objective economic emission dispatch problem. Energy 259:124876. https://doi.org/10.1016/j.energy.2022.124876

Zhang Q, Li H (2007) MOEA/D: A Multiobjective Evolutionary Algorithm Based on Decomposition. IEEE Trans Evol Comput 11:712–731. https://doi.org/10.1109/TEVC.2007.892759